International Journal of Non-Linear Mechanics 71 (2015) 52–62

Contents lists available at ScienceDirect

International Journal of Non-Linear Mechanics

journal homepage: www.elsevier.com/locate/nlm

Numerical characterization of effective fully coupled thermo-electro-magneto-viscoelastic-plastic response of smart composites

Tian Tang *, Sergio D. Felicelli

Department of Mechanical Engineering, The University of Akron, Akron, OH 44325, USA

ARTICLE INFO

Article history:
Received 21 November 2014
Received in revised form
11 January 2015
Accepted 26 January 2015
Available online 3 February 2015

Keywords:
Thermo-electro-magneto-viscoelastic-plastic response
Smart composites
Micromechanics
VAMUCH

ABSTRACT

The focus of the present paper is to construct a general purpose micromechanics model to predict the effective fully coupled time-dependent and non-linear multiphysics responses of smart composites. The present model is established on the basis of the variational asymptotic method and implemented using the finite element method. In light of the time-dependent and non-linear characteristics of composites, an incremental procedure in conjunction with an instantaneous tangential electromagnetomechanical matrix of composites was established. The accuracy of the proposed model was verified through the comparison with ABAQUS results. Finally, a numerical example was employed to demonstrate the capability of the proposed model.

1. Introduction

The smart composite consisting of piezoelectric and piezomagnetic constituents displays a magneto-electric coupling effect that is absent in constituents [1–9]. The magneto-electric coupling effect created by the interaction of piezoelectric phases and piezomagnetic phases has recently been extensively investigated due to their broad engineering applications [10–12]. Since the piezoelectric and piezomagnetic ceramics are brittle and susceptible to fracture, adding a polymer or metallic alloy matrix into the two-phase electromagnetoelastic composite will increase the ductility and formability of the composites. To date, several investigations have been conducted for the response of smart composites containing metallic phases. For example, Bednarcyk [13] developed a micro-macro theory to predict the fully coupled electro-magneto-thermo-elasto-plastic behavior of arbitrary composite laminates using Generalized Method of Cell (GMC). Due to the introduction of linear viscoelastic polymer matrix, the composites exhibit time dependent behavior [14]. The reports that are involved in the response of smart composites containing both metallic phases and viscoelastic phases is still limited. Therefore, there is a need to develop an efficient micromechanical tool for the analysis and design of such composites.

The goal of this paper is to develop a general purpose micromechanics model for predicting the time-dependent, non-linear, and multiphysics response of smart composites. In light of the time-dependent characteristics and non-linearity of constitutive relations, an incremental procedure associated with instantaneous tangential electromechanical matrix was established based on the micromechanics framework VAMUCH [15]. In order to demonstrate the capability, a smart composites consisting of metallic phase, piezoelectric material, piezomagnetic material, and linear viscoelastic matrix was analyzed using the proposed model.

2. Incremental constitutive equations of materials

2.1. Constitutive equations for linear thermo-viscoelastic polymer

Considering the linear thermo-viscoelastic polymer having no history of stress and deformation before time $t=0$, then based on the Boltzmann superposition principle, the constitutive equations for the linear thermo-viscoelastic polymer can be expressed in the time domain in the following way:

$$\sigma_{ij}(t) = \int_0^t \left[B_{ijkl}(t-\tau)\dot{\varepsilon}_{kl}(\tau) + \beta_{ij}(t-\tau)\dot{\theta}(\tau)\right] d\tau \tag{1a}$$

$$D_i(t) = \int_0^t \left[k_{ij}(t-\tau)\dot{E}_j(\tau) + p_i(t-\tau)\dot{\theta}(\tau)\right] d\tau \tag{1b}$$

* Corresponding author. Tel.: +1 330 972 7672.
E-mail address: tiantang1991@gmail.com (T. Tang).

http://dx.doi.org/10.1016/j.ijnonlinmec.2015.01.008
0020-7462/

$$B_i(t) = \int_0^t \left[\mu_{ij}(t-\tau)\dot{H}_j(\tau) + m_i(t-\tau)\dot{\theta}(\tau)\right] d\tau \tag{1c}$$

where $B_{ijkl}(t)$, $k_{ij}(t)$, and $\mu_{ij}(t)$ are the stress relaxation stiffness, dielectric tensor, and magnetic permeability tensor, respectively; $\dot{\varepsilon}_{kl}(\tau)$ is the strain rate; and $\dot{E}_j(\tau)$ and $\dot{H}_j(\tau)$ are the electric field rate and magnetic field rate, respectively; $\dot{\theta}(\tau)$ is the temperature change rate; $\sigma_{ij}(t)$, $D_i(t)$, and $B_i(t)$ are the instantaneous stress tensor, electrical displacement vector, and magnetic induction vector, respectively; $\beta_{ij}(t)$, $p_i(t)$, and $m_i(t)$ are the instantaneous thermal stress tensor, pyroelectric vector, and pyromagnetic vector, respectively. Note that $\beta_{ij}(t) = -B_{ijkl}(t)\alpha_{kl}$ with α_{kl} being thermal expansion coefficients. In this study, the α_{kl} is assumed to be constant.

According to the time–temperature superposition principle [16], the real time t has to be replaced with reduced time ξ in order to account for the variation of material's properties of polymer with temperature. Hence, Eq. (1a)–(1c) can be rewritten as

$$\sigma_{ij}(t) = \int_0^t \left[B_{ijkl}(\xi-\xi')\dot{\varepsilon}_{kl}(\xi') + \beta_{ij}(\xi-\xi')\dot{\theta}(\xi')\right] d\xi' \tag{2a}$$

$$D_i(t) = \int_0^t \left[k_{ij}(\xi-\xi')\dot{E}_j(\xi') + p_i(\xi-\xi')\dot{\theta}(\xi')\right] d\xi' \tag{2b}$$

$$B_i(t) = \int_0^t \left[\mu_{ij}(\xi-\xi')\dot{H}_j(\xi') + m_i(\xi-\xi')\dot{\theta}(\xi')\right] d\xi' \tag{2c}$$

The reduced time $\xi = \xi(t)$ is defined by

$$\xi(t) = \int_0^t \frac{dt'}{a_T} \tag{3}$$

where a_T is a time-scale shift factor, and $\xi' = \xi(\tau)$.

As pointed out by Pyatigorets et al. [17], since the corresponding value of real time t can be found for each value of reduced time ξ and vice versa, the stress and strain in the reduced time domain can be replaced with their values found for the corresponding real time, such that

$$\sigma_{ij}(\xi) \equiv \sigma_{ij}(\xi(t)) \equiv \sigma_{ij}(t), \quad \varepsilon_{ij}(\xi) \equiv \varepsilon_{ij}(\xi(t)) \equiv \varepsilon_{ij}(t) \tag{4}$$

Hence, the Eq. (2a)–(2c) can be simplified as

$$\sigma_{ij}(t) = \int_0^t \left[B_{ijkl}(\xi(t)-\xi(\tau))\dot{\varepsilon}_{kl}(\tau) + \beta_{ij}(\xi(t)-\xi(\tau))\dot{\theta}(\tau)\right] d\tau \tag{5a}$$

$$D_i(t) = \int_0^t \left[k_{ij}(\xi(t)-\xi(\tau))\dot{E}_j(\tau) + p_i(\xi(t)-\xi(\tau))\dot{\theta}(\tau)\right] d\tau \tag{5b}$$

$$B_i(t) = \int_0^t \left[\mu_{ij}(\xi(t)-\xi(\tau))\dot{H}_j(\tau) + m_i(\xi(t)-\xi(\tau))\dot{\theta}(\tau)\right] d\tau \tag{5c}$$

In light of the non-linear, time dependent, and multiphysics response of the composites, our analysis need to be incremental. The incremental formulations of Eq. (5a)–(5c) can be expressed as

$$\begin{aligned}\Delta\sigma_{ij}(t) &= \sigma_{ij}(t+\Delta t) - \sigma_{ij}(t)\\ &= \int_t^{t+\Delta t} \left[B_{ijkl}(\xi(t+\Delta t)-\xi(\tau))\dot{\varepsilon}_{kl}(\tau) + \beta_{ij}(\xi(t+\Delta t)-\xi(\tau))\dot{\theta}(\tau)\right] d\tau\\ &\quad + \int_0^t \left[B_{ijkl}(\xi(t+\Delta t)-\xi(\tau))\dot{\varepsilon}_{kl}(\tau) + \beta_{ij}(\xi(t+\Delta t)-\xi(\tau))\dot{\theta}(\tau)\right] d\tau\\ &\quad - \int_0^t \left[B_{ijkl}(\xi(t)-\xi(\tau))\dot{\varepsilon}_{kl}(\tau) + \beta_{ij}(\xi(t)-\xi(\tau))\dot{\theta}(\tau)\right] d\tau\end{aligned} \tag{6a}$$

$$\begin{aligned}\Delta D_i(t) &= D_i(t+\Delta t) - D_i(t)\\ &= \int_t^{t+\Delta t} \left[k_{ij}(\xi(t+\Delta t)-\xi(\tau))\dot{E}_j(\tau) + p_i(\xi(t+\Delta t)-\xi(\tau))\dot{\theta}(\tau)\right] d\tau\\ &\quad + \int_0^t \left[k_{ij}(\xi(t+\Delta t)-\xi(\tau))\dot{E}_j(\tau) + p_i(\xi(t+\Delta t)-\xi(\tau))\dot{\theta}(\tau)\right] d\tau\\ &\quad - \int_0^t \left[k_{ij}(\xi(t)-\xi(\tau))\dot{E}_j(\tau) + p_i(\xi(t)-\xi(\tau))\dot{\theta}(\tau)\right] d\tau\end{aligned} \tag{6b}$$

$$\begin{aligned}\Delta B_i(t) &= B_i(t+\Delta t) - B_i(t)\\ &= \int_t^{t+\Delta t} \left[\mu_{ij}(\xi(t+\Delta t)-\xi(\tau))\dot{H}_j(\tau) + m_i(\xi(t+\Delta t)-\xi(\tau))\dot{\theta}(\tau)\right] d\tau\\ &\quad - \int_0^t \left[\mu_{ij}(\xi(t+\Delta t)-\xi(\tau))\dot{H}_j(\tau) + m_i(\xi(t+\Delta t)-\xi(\tau))\dot{\theta}(\tau)\right] d\tau\\ &\quad - \int_0^t \left[\mu_{ij}(\xi(t)-\xi(\tau))\dot{H}_j(\tau) + m_i(\xi(t)-\xi(\tau))\dot{\theta}(\tau)\right] d\tau\end{aligned} \tag{6c}$$

Although the strain rate, electrical field rate, and magnetic field rate are not necessarily constant in the whole time domain, it is reasonable to assume that the strain rate, electrical field rate, and magnetic field rate are kept constant during each time increment Δt. The temperature change rate can be kept uniform in the whole composites. Then, the Eq. (6a)–(6c) can be rephrased as

$$\Delta\sigma_{ij}(t) = L_{ijkl}(t)\Delta\varepsilon_{kl}(t) + \gamma_{ij}(t)\Delta\theta(t) + \omega_{ij}(t) \tag{7a}$$

with

$$\begin{aligned}L_{ijkl}(t) &= \frac{1}{\Delta t}\int_t^{t+\Delta t} B_{ijkl}[\xi(t+\Delta t)-\xi(\tau)]d\tau\\ \gamma_{ij}(t) &= \frac{1}{\Delta t}\left(\int_t^{t+\Delta t} \beta_{ij}[\xi(t+\Delta t)-\xi(\tau)]d\tau\right)\\ \omega_{ij}(t) &= \int_0^t \left[B_{ijkl}(\xi(t+\Delta t)-\xi(\tau)) - B_{ijkl}(\xi(t)-\xi(\tau))\right]\dot{\varepsilon}_{kl}(\tau)\, d\tau\\ &\quad + \int_0^t \left[\beta_{ij}(\xi(t+\Delta t)-\xi(\tau)) - \beta_{ij}(\xi(t)-\xi(\tau))\right]\dot{\theta}(\tau)d\tau\end{aligned}$$

$$-\Delta D_i(t) = -K_{ik}(t)\Delta E_k(t) - P_i(t)\Delta\theta - \varpi_i(t) \tag{7b}$$

with

$$\begin{aligned}K_{ik}(t) &= \frac{1}{\Delta t}\int_t^{t+\Delta t} k_{ik}(\xi(t+\Delta t)-\xi(\tau))d\tau\\ P_i(t) &= \frac{1}{\Delta t}\left(\int_t^{t+\Delta t} p_i(\xi(t+\Delta t)-\xi(\tau))d\tau\right)\\ \varpi_i(t) &= \int_0^t \left[k_{ij}(\xi(t+\Delta t)-\xi(\tau)) - k_{ij}(\xi(t)-\xi(\tau))\right]\dot{E}_j(\tau)\, d\tau\\ &\quad + \int_0^t \left[p_i(\xi(t+\Delta t)-\xi(\tau)) - p_i(\xi(t)-\xi(\tau))\right]\dot{\theta}(\tau)d\tau\end{aligned}$$

$$-\Delta B_i(t) = -N_{ik}(t)\Delta H_k(t) - M_i(t)\Delta\theta - \Psi_i(t) \tag{7c}$$

with

$$\begin{aligned}N_{ik}(t) &= \frac{1}{\Delta t}\int_t^{t+\Delta t} \mu_{ik}(\xi(t+\Delta t)-\xi(\tau))d\tau\\ M_i(t) &= \frac{1}{\Delta t}\left(\int_t^{t+\Delta t} m_i(\xi(t+\Delta t)-\xi(\tau))d\tau\right)\\ \Psi_i(t) &= \int_0^t \left[\mu_{ij}(\xi(t+\Delta t)-\xi(\tau)) - \mu_{ij}(\xi(t)-\xi(\tau))\right]\dot{H}_j(\tau)\, d\tau\\ &\quad + \int_0^t [m_i(\xi(t+\Delta t)-\xi(\tau)) - m_i(\xi(t)-\xi(\tau))]\dot{\theta}(\tau)d\tau\end{aligned}$$

2.2. Constitutive equations for piezoelectric-piezomagnetic materials

The elastic and the dielectric responses are coupled in piezoelectric materials where the mechanical variables of stress, and strain are related to each other as well as to the electric variables of electric field and electric displacement. The coupling between mechanical and electric fields is described by piezoelectric coefficients. The linear rate independent coupled constitutive equations of piezoelectric materials are given by

$$\sigma_{ij} = C^e_{ijkl}\varepsilon_{kl} - e_{ijk}E_k - q_{ijk}H_k + \beta_{ij}\theta \tag{8a}$$

$$D_i = e_{ikl}\varepsilon_{kl} + k_{ik}E_k + a_{ik}H_k + p_i\theta \tag{8b}$$

$$B_i = e_{ikl}\varepsilon_{kl} + a_{ik}E_k + \mu_{ik}H_k + m_i\theta \tag{8c}$$

where C^e_{ijkl}, e_{ijk}, q_{ijk}, and β_{ij} are the elastic, piezoelectric, piezomagnetic and thermal stress tensors, respectively (note that $\beta_{ij} = -C^e_{ijkl}\alpha_{kl}$ with α_{kl} as the thermal expansion strain tensor); k_{ik}, a_{ik}, and μ_{ik} are the dielectric, magnetoelectric, and magnetic permeability tensors, respectively; E_k and H_k are the electrical field and magnetic field vectors, respectively.

The incremental form of Eq. (8a)–(8c) is expressed as

$$\Delta\sigma_{ij} = C^e_{ijkl}\Delta\varepsilon_{kl} - e_{ijk}\Delta E_k - q_{ijk}\Delta H_k + \beta_{ij}\Delta\theta \tag{9a}$$

$$-\Delta D_i = -e_{ikl}\Delta\varepsilon_{kl} - k_{ik}\Delta E_k - a_{ik}\Delta H_k - p_i\Delta\theta \tag{9b}$$

$$-\Delta B_i = -e_{ikl}\Delta\varepsilon_{kl} - a_{ik}\Delta E_j - \mu_{ik}\Delta H_k - m_i\Delta\theta \tag{9c}$$

2.3. Constitutive equations for metal

The incremental stress–strain relation of metals can be expressed as

$$\Delta\sigma_{ij} = C_{ijkl}\Delta\varepsilon_{kl} + \beta_{ij}\Delta\theta \tag{10a}$$

$$-\Delta D_i = -k_{ik}\Delta E_k - p_i\Delta\theta \tag{10b}$$

$$-\Delta B_i = \mu_{ik}\Delta H_k - m_i\Delta\theta \tag{10c}$$

where C_{ijkl} are the components of the time independent fourth-order instantaneous tangent stiffness tensor which is the elastic stiffness tensor C^e_{ijkl} when the stress state of the material point is below yielding and the elastoplastic tangent stiffness tensor C^{ep}_{ijkl} when the stress state of the material point beyond yielding. According to the classical plasticity theory, the C^{ep}_{ijkl} is given by

$$C^{ep}_{ijkl} = \left(C^e_{ijkl} - \frac{C^e_{ijmn}(\partial f/\partial\sigma_{mn})(\partial f/\partial\sigma_{pq})C^e_{pqkl}}{(\partial f/\partial\sigma_{rs})C^e_{rstu}(\partial f/\partial\sigma_{tu}) - (\partial f/\partial p)\sqrt{(2/3)(\partial f/\partial\sigma_{dw})(\partial f/\partial\sigma_{dw})}} \right) \tag{11}$$

where f and p in Eq. (8a)–(8c) are yielding function and effective plastic strain, respectively.

3. Micromechanics formulations

Consider the smart composites with periodic microstructure as shown in Fig. 1. Two coordinate systems including $x = (x_1,\ x_2,\ x_3)$ and $y = (y_1,\ y_2,\ y_3)$ are adopted to facilitate the micromechanics formulations. We use x_i as the global coordinates to describe the macroscopic structure and y_i parallel to x_i as the local coordinates to describe the UC (here and throughout the paper, Latin indices assume 1, 2, and 3 and repeated indices are summed over their range except where explicitly indicated). We choose the origin of the local coordinate system y_i to be the geometric center of UC.

3.1. Genera incremental formulations of the smart composite and its constituents

The incremental formulations of polymer, piezoelectric-piezomagnetic materials, and metal described by Eqs. (7a)–(7c), (9a)–(9c), and (10a)–(10c) can be extended to the following general incremental formulations:

$$\Delta\sigma_{ij}(t) = M_{ijkl}(t)\Delta\varepsilon_{kl}(t) - e_{ijk}(t)\Delta E_k(t) - q_{ijk}(t)\Delta H_k(t) + \beta_{ij}(t)\Delta\theta(t) + \omega_{ij}(t) \tag{12a}$$

$$-\Delta D_i(t) = -e_{ikl}(t)\Delta\varepsilon_{kl}(t) - k_{ik}(t)\Delta E_k - a_{ik}(t)\Delta H_k(t) - p_i(t)\Delta\theta(t) - \varpi_i(t) \tag{12b}$$

$$-\Delta B_i(t) = -e_{ikl}(t)\Delta\varepsilon_{kl}(t) - a_{ik}(t)\Delta E_k - \mu_{ik}(t)\Delta H_k(t) - m_i(t)\Delta\theta(t) - \Psi_i(t) \tag{12c}$$

where

$$M_{ijkl}(t) = \begin{cases} L_{ijkl}(t) & \text{for polymer materials} \\ C^e_{ijkl} & \text{for piezoelectric materials} \\ C^e_{ijkl} & \text{for piezomagnetic materials} \\ C^e_{ijkl} \text{ or } C^{ep}_{ijkl} & \text{for metal} \end{cases}$$

$$e_{ijk}(t) = \begin{cases} 0 & \text{for polymer materials} \\ e_{ijk} & \text{for piezoelectric materials} \\ 0 & \text{for piezomagnetic materials} \\ 0 & \text{for metal} \end{cases}$$

$$q_{ijk}(t) = \begin{cases} 0 & \text{for polymer materials} \\ 0 & \text{for piezoelectric materials} \\ q_{ijk} & \text{for piezomagnetic materials} \\ 0 & \text{for metal} \end{cases}$$

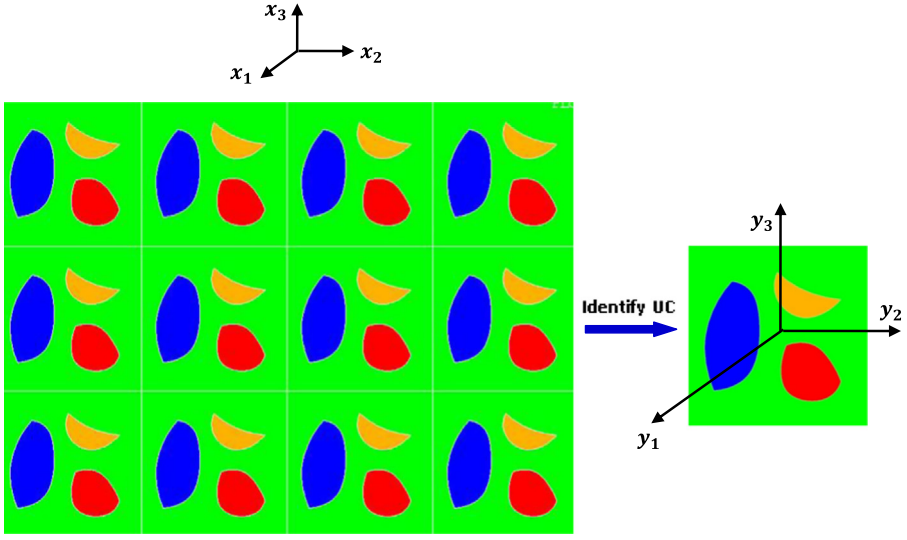

Fig. 1. A sketch of periodic heterogeneous materials (only two-dimensional (2D) UC is drawn for clarity).

$$k_{ik}(t)=\begin{cases}K_{ik}(t) & \text{for polymer materials}\\ k_{ik} & \text{for piezoelectric materials}\\ k_{ik} & \text{for piezomagnetic materials}\\ k_{ik} & \text{for metal}\end{cases}$$

$$\mu_{ik}(t)=\begin{cases}N_{ik}(t) & \text{for polymer materials}\\ \mu_{ik} & \text{for piezoelectric materials}\\ \mu_{ik} & \text{for piezomagnetic materials}\\ \mu_{ik} & \text{for metal}\end{cases}$$

$$\beta_{ij}(t)=\begin{cases}\gamma_{ij}(t) & \text{for polymer materials}\\ \beta_{ij} & \text{for piezoelectric materials}\\ \beta_{ij} & \text{for piezomagnetic materials}\\ \beta_{ij} & \text{for metal}\end{cases}$$

$$\omega_{ij}(t)=\begin{cases}\omega_{ij}(t) & \text{for polymer materials}\\ 0 & \text{for piezoelectric materials}\\ 0 & \text{for piezomagnetic materials}\\ 0 & \text{for metal}\end{cases}$$

$$\varpi_i(t)=\begin{cases}\varpi_{ij}(t) & \text{for polymer materials}\\ 0 & \text{for piezoelectric materials}\\ 0 & \text{for piezomagnetic materials}\\ 0 & \text{for metal}\end{cases}$$

$$\Psi_i(t)=\begin{cases}\Psi_i(t) & \text{for polymer materials}\\ 0 & \text{for piezoelectric materials}\\ 0 & \text{for piezomagnetic materials}\\ 0 & \text{for metal}\end{cases}$$

Note that $a_{ik}(t)$, $p_i(t)$, and $m_i(t)$ are absent in individual material constituents but existing in composites.

Let us define the vectors ΔX and ΔY as follows:

$$\Delta X=[\Delta\sigma_{11}(t)\ \Delta\sigma_{12}(t)\ \Delta\sigma_{22}(t)\ \Delta\sigma_{13}(t)\ \Delta\sigma_{23}(t)\ \Delta\sigma_{33}(t)\ -\Delta D_1(t)\ -\Delta D_2(t)\ -\Delta D_3(t)\ -\Delta B_1(t)\ -\Delta B_2(t)\ -\Delta B_3(t)]^T \tag{13}$$

$$\Delta Y=[\Delta\varepsilon_{11}(t)\ \Delta\varepsilon_{12}(t)\ \Delta\varepsilon_{22}(t)\ \Delta\varepsilon_{13}(t)\ \Delta\varepsilon_{23}(t)\ \Delta\varepsilon_{33}(t)\ \Delta E_1(t)\ \Delta E_2(t)\ \Delta E_3(t)\ \Delta H_1(t)\ \Delta H_2(t)\ \Delta H_3(t)]^T \tag{14}$$

The compact matrix form of Eq. (12a)–(12c) is given by

$$\Delta X=R\Delta Y+\eta\Delta\theta(t)+\mathcal{K} \tag{15}$$

where $\Delta\theta(t)$ is the instantaneous increment of temperature change. R is a 12×12 instantaneous material matrix and expressed as

$$R=\begin{bmatrix}M & -e & -q\\ -e^{\mathrm{T}} & -k & -a\\ -q^{\mathrm{T}} & -a^{\mathrm{T}} & -\mu\end{bmatrix} \tag{16}$$

where M is a 6×6 submatrix for $M_{ijkl}(t)$ coefficients; e is a 6×3 submatrix for $e_{ijk}(t)$ coefficients; q is a 6×3 submatrix for $q_{ijk}(t)$ coefficients; k is a 3×3 submatrix for $k_{ik}(t)$ coefficients; a is a 3×3 submatrix for $a_{ik}(t)$ coefficients; and μ is a 3×3 submatrix for $\mu_{ijk}(t)$ coefficients. The superscript "T" means transpose matrix.

In Eq. (15), η is a 12×1 matrix and expressed as

$$\eta=\begin{Bmatrix}\beta\\ -p\\ -m\end{Bmatrix} \tag{17}$$

where β is a 6×1 submatrix for $\beta_{ij}(t)$ coefficients; m is a 3×1 submatrix for $m_i(t)$ coefficients; and p is a 3×1 submatrix for $p_i(t)$ coefficients.

In Eq. (15), $\mathcal{K}$ is a 12×1 matrix and expressed as

$$\mathcal{K}=\begin{Bmatrix}\omega\\ \varpi\\ \Psi\end{Bmatrix} \tag{18}$$

where ω is a 6×1 submatrix for $\omega_{ij}(t)$ coefficients; ϖ is a 3×1 submatrix for $\varpi_i(t)$ coefficients; and Ψ is a 3×1 submatrix for $\Psi_i(t)$ coefficients.

The effective instantaneous thermo-electro-magneto-viscoelastic-plastic coefficients of smart composite materials can be defined in the following two ways:

$$\Delta\overline{X}=R^*\Delta\overline{Y}+\eta^*\Delta\theta(t)+\mathcal{K}^* \tag{19}$$

$$\frac{1}{\Omega}\int_{\Omega}\left[\frac{1}{2}\Delta Y^{\mathrm{T}}R\Delta Y+\Delta Y^{\mathrm{T}}\eta\Delta\theta(t)+\Delta Y^{\mathrm{T}}\mathcal{K}+\frac{1}{2}G\Delta\theta(t)+\frac{1}{2}c_v\frac{\Delta\theta(t)^2}{T_0}+\frac{1}{2}h_v\right]d\Omega$$
$$=\frac{1}{2}\Delta\overline{Y}^{\mathrm{T}}R^*\Delta\overline{Y}+\Delta\overline{Y}^{\mathrm{T}}\eta^*\Delta\theta(t)+\Delta\overline{Y}^{\mathrm{T}}\mathcal{K}^*+\frac{1}{2}G^*\Delta\theta(t)+\frac{1}{2}c_v^*\frac{\Delta\theta(t)^2}{T_0}+\frac{1}{2}h_v^* \tag{20}$$

where G is the energy change per unit temperature; c_v is the specific heat per unit volume at constant volume; T_0 is the reference temperature at which the constituent material is stress free; h_v is the energy change similar to c_v. In Eqs. (19)–(20), "over-bar" indicates variables which are used in the macroscopic analysis of homogenized materials, and superscripts "*" denote the effective properties whose calculations are determined by the micromechanics model one employs. Ω is the volume of unit cell.

3.2. VAMUCH model

The total change of potential energy of the composites can be formulated as

$$\Pi=\int_{\mathscr{R}}\langle\frac{1}{2}\Delta Y^{\mathrm{T}}R\Delta Y+\Delta Y^{\mathrm{T}}\eta\Delta\theta(\mathrm{t})+\Delta Y^{\mathrm{T}}\mathcal{K}+\frac{1}{2}G\Delta\theta(t)+\frac{1}{2}c_v\frac{\Delta\theta(t)^2}{T_0}+\frac{1}{2}h_v\rangle d\mathscr{R} \tag{21}$$

with

$$\Delta\varepsilon_{ij}(t;\boldsymbol{x};\boldsymbol{y})=\frac{1}{2}\left[\frac{\partial\Delta u_i(t;\boldsymbol{x};\boldsymbol{y})}{\partial y_j}+\frac{\partial\Delta u_j(t;\boldsymbol{x};\boldsymbol{y})}{\partial y_i}\right]\equiv\Delta u_{(i|j)} \tag{22}$$

$$\Delta E_i(t;\boldsymbol{x};\boldsymbol{y})=-\frac{\partial\Delta\varnothing^e(t;\boldsymbol{x};\boldsymbol{y})}{\partial y_i} \tag{23}$$

$$\Delta H_i(t;\boldsymbol{x};\boldsymbol{y})=-\frac{\partial\Delta\varnothing^m(t;\boldsymbol{x};\boldsymbol{y})}{\partial y_i} \tag{24}$$

where Δu_i, $\Delta\varnothing^e$, and $\Delta\varnothing^m$ are the increments of displacement vector, electrical potential, and magnetic potential, respectively. Since Δu_i, $\Delta\varnothing^e$, and $\Delta\varnothing^m$ are continuous functions at the interfaces between adjacent unit cells, we have

$$\begin{aligned}&\Delta u_i(t;x_1,x_2,x_3;\ d_1/2,y_2,y_3)=\Delta u_i(t;x_1+d_1,x_2,x_3;\ -d_1/2,y_2,y_3)\\ &\Delta u_i(t;x_1,x_2,x_3;\ y_1,d_2/2,y_3)=\Delta u_i(t;x_1,x_2+d_2,n_3;\ y_1,-d_2/2,y_3)\\ &\Delta u_i(t;x_1,x_2,x_3;\ y_1,y_2,d_3/2)=\Delta u_i(t;x_1,x_2,x_3+d_3;\ y_1,y_2,-d_3/2)\end{aligned} \tag{25}$$

$$\begin{aligned}&\Delta\varnothing^e(t;x_1,x_2,x_3;\ d_1/2,y_2,y_3)=\Delta\varnothing^e(t;x_1+d_1,x_2,x_3;\ -d_1/2,y_2,y_3)\\ &\Delta\varnothing^e(t;x_1,x_2,x_3;\ y_1,d_2/2,y_3)=\Delta\varnothing^e(t;x_1,x_2+d_2,n_3;\ y_1,-d_2/2,y_3)\\ &\Delta\varnothing^e(t;x_1,x_2,x_3;\ y_1,y_2,d_3/2)=\Delta\varnothing^e(t;x_1,x_2,x_3+d_3;\ y_1,y_2,-d_3/2)\end{aligned} \tag{26}$$

$$\Delta\varnothing^m(t;x_1,x_2,x_3;\ d_1/2,y_2,y_3)=\Delta\varnothing^m(t;x_1+d_1,x_2,x_3;\ -d_1/2,y_2,y_3)$$

$$\Delta\varnothing^m(t;x_1,x_2,x_3;\ y_1,d_2/2,y_3)=\Delta\varnothing^m(t;x_1,x_2+d_2,n_3;\ y_1,-d_2/2,y_3)$$
$$\Delta\varnothing^m(t;x_1,x_2,x_3;\ y_1,y_2,d_3/2)=\Delta\varnothing^m(t;x_1,x_2,x_3+d_3;\ y_1,y_2,-d_3/2) \tag{27}$$

In Eq. (28) and throughout this paper, the angle bracket denotes average over the domain of the UC, that is

$$\langle f\rangle=\frac{1}{\Omega}\int_\Omega f d\Omega \tag{28}$$

with Ω denoting the unit cell domain.

Because Δu_i, $\Delta\varnothing^e$, and $\Delta\varnothing^m$ are continuous function defined in the UC, we can denote the average of Δu_i, $\Delta\varnothing^e$, and $\Delta\varnothing^m$ over the UC as Δv_i, $\Delta\varphi^e$, and $\Delta\varphi^m$, respectively, such that

$$\Delta v_i=\langle\Delta u_i\rangle\quad \Delta\varphi^e=\langle\Delta\varnothing^e\rangle\quad \Delta\varphi^m=\langle\Delta\varnothing^m\rangle \tag{36}$$

Taking advantage of the method of change of variables for Δu_i, $\Delta\varnothing^e$, and $\Delta\varnothing^m$, we can obtain

$$\Delta u_i(t;\boldsymbol{x};\boldsymbol{y})=\Delta v_i(t;\boldsymbol{x})+y_j\frac{\partial\Delta v_i}{\partial x_j}+\chi_i(t;\boldsymbol{x};\boldsymbol{y}) \tag{37a}$$

$$\Delta\varnothing^e(t;\boldsymbol{x};\boldsymbol{y})=\Delta\varphi^e(t;\boldsymbol{x})+y_j\frac{\partial\Delta\varphi^e}{\partial x_j}+\zeta^e(t;\boldsymbol{x};\boldsymbol{y}) \tag{37b}$$

$$\Delta\varnothing^m(t;\boldsymbol{x};\boldsymbol{y})=\Delta\varphi^m(t;\boldsymbol{x})+y_j\frac{\partial\Delta\varphi^m}{\partial x_j}+\zeta^m(t;\boldsymbol{x};\boldsymbol{y}) \tag{37c}$$

where χ_i, ζ^e, and ζ^m are the fluctuation functions for the displacement changes, electric potential changes, and magnetic potential change, respectively. When the origin of the local coordinate system is chosen to be the center of UC, we have,

$$\langle\chi_i\rangle=0\quad\langle\zeta^e=0\rangle\quad\langle\zeta^m\rangle=0 \tag{38}$$

Using the technique of Lagrange multipliers in conjunction with Eqs. (37)–(38), we finally obtain a stationary value problem defined over UC for χ_i, ζ^e, ζ^m according to the variational asymptotic method [18], such that

$$\begin{aligned}J_\Omega=\langle&\frac{1}{2}\Delta Y^{\mathrm T}R\Delta Y+\Delta Y^{\mathrm T}\eta\Delta\theta(t)+\Delta Y^{\mathrm T}\mathcal{K}+\frac{1}{2}G\Delta\theta(t)+\frac{1}{2}c_v\frac{\Delta\theta(t)^2}{T_0}+\frac{1}{2}h_v\rangle\\&+\sum_{j=1}^{3}\int_{S_j}\lambda_{ij}\left(\chi_i^{+j}-\chi_i^{-j}\right)dS_j+\sum_{j=1}^{3}\int_{S_j}g_i\left(\zeta^e_{+j}-\zeta^e_{-j}\right)dS_j\\&+\sum_{j=1}^{3}\int_{S_j}h_i\left(\zeta^m_{+j}-\zeta^m_{-j}\right)dS_j\end{aligned} \tag{39}$$

with

$$\chi_i^{+j}=\chi_i|_{y_j=d_j/2}\quad\chi_i^{-j}=\chi_i|_{y_j=-d_j/2}\quad\text{for } j=1,2,3$$
$$\zeta^e_{+j}=\zeta^e|_{y_j=d_j/2}\quad\zeta^e_{-j}=\zeta^e|_{y_j=-d_j/2}\quad\text{for } j=1,2,3$$
$$\zeta^m_{+j}=\zeta^m|_{y_j=d_j/2}\quad\zeta^m_{-j}=\zeta^m|_{y_j=-d_j/2}\quad\text{for } j=1,2,3$$

Matrix ΔY are given by

$$\Delta Y=\Delta\overline{Y}+\Delta Y_1 \tag{40}$$

with

$$\begin{aligned}\Delta\overline{Y}=\big[&\Delta\bar\varepsilon_{11}(t)\Delta\bar\varepsilon_{12}(t)\Delta\bar\varepsilon_{22}(t)\Delta\bar\varepsilon_{13}(t)\Delta\bar\varepsilon_{23}(t)\Delta\bar\varepsilon_{33}(t)\Delta\overline{E}_1(t)\\&\Delta\overline{E}_2(t)\Delta\overline{E}_3(t)\Delta\overline{H}_1(t)\Delta\overline{H}_2(t)\Delta\overline{H}_3(t)\big]^{\mathrm T}\end{aligned} \tag{41}$$

$$\begin{aligned}\Delta Y_1=\Big[&\Delta\hat\varepsilon_{11}(t)\Delta\hat\varepsilon_{12}(t)\Delta\hat\varepsilon_{22}(t)\Delta\hat\varepsilon_{13}(t)\Delta\hat\varepsilon_{23}(t)\Delta\hat\varepsilon_{33}(t)\Delta\hat{E}_1(t)\\&\Delta\hat{E}_2(t)\Delta\hat{E}_3(t)\Delta\hat{H}_1(t)\Delta\hat{H}_2(t)\Delta\hat{H}_3(t)\Big]^{\mathrm T}\end{aligned} \tag{42}$$

where

$$\Delta\bar\varepsilon_{ij}(t)=\frac{1}{2}\left[\frac{\partial\Delta v_i(t;\boldsymbol{x})}{\partial x_j}+\frac{\partial\Delta v_j(t;\boldsymbol{x})}{\partial x_i}\right] \tag{43a}$$

$$\Delta\overline{E}_i(t)=-\frac{\partial\Delta\zeta^e(t;\boldsymbol{x})}{\partial x_i} \tag{43b}$$

$$\Delta\overline{H}_i(t)=-\frac{\partial\Delta\zeta^m(t;\boldsymbol{x})}{\partial x_i} \tag{43c}$$

$$\Delta\hat\varepsilon_{ij}(t)=\frac{1}{2}\left[\frac{\partial\chi_i(t;\boldsymbol{x};\boldsymbol{y})}{\partial y_j}+\frac{\partial\chi_j(t;\boldsymbol{x};\boldsymbol{y})}{\partial y_i}\right] \tag{44a}$$

$$\Delta\hat{E}_i(t)=-\frac{\partial\Delta\zeta^e(t;\boldsymbol{x};\boldsymbol{y})}{\partial y_i} \tag{44b}$$

$$\Delta\hat{H}_i(t)=-\frac{\partial\Delta\zeta^m(t;\boldsymbol{x};\boldsymbol{y})}{\partial y_i} \tag{44c}$$

In order to avoid the difficulties associated with the unknowns introduced by the Lagrange multipliers, we reformulate the stationary problem of the functional in Eq. (39) as the minimum value of the following functional:

$$\Pi_\Omega=\frac{1}{\Omega}\int_\Omega\left[\frac{1}{2}\Delta Y^{\mathrm T}R\Delta Y+\Delta Y^{\mathrm T}\eta\Delta\theta(t)+\Delta Y^{\mathrm T}\mathcal{K}+\frac{1}{2}G\Delta\theta(t)+\frac{1}{2}c_v\frac{\theta(t)^2}{T_0}+\frac{1}{2}h_v\right]d\Omega \tag{45}$$

under the following constraints:

$$\chi_i^{+j}=\chi_i^{-j}\quad\zeta^e_{+j}=\zeta^e_{-j}\quad\zeta^m_{+j}=\zeta^m_{-j}\quad\text{for } i,j=1,2,3$$

Introduce the following matrix form:

$$\Delta Y_1=\begin{bmatrix}\frac{\partial}{\partial y_1}&0&0&0&0\\ \frac{\partial}{\partial y_2}&\frac{\partial}{\partial y_1}&0&0&0\\ 0&\frac{\partial}{\partial y_2}&0&0&0\\ \frac{\partial}{\partial y_3}&0&\frac{\partial}{\partial y_1}&0&0\\ 0&\frac{\partial}{\partial y_2}&\frac{\partial}{\partial y_3}&0&0\\ 0&0&\frac{\partial}{\partial y_3}&0&0\\ 0&0&0&-\frac{\partial}{\partial y_1}&0\\ 0&0&0&-\frac{\partial}{\partial y_2}&0\\ 0&0&0&-\frac{\partial}{\partial y_3}&0\\ 0&0&0&0&-\frac{\partial}{\partial y_1}\\ 0&0&0&0&-\frac{\partial}{\partial y_2}\\ 0&0&0&0&-\frac{\partial}{\partial y_3}\end{bmatrix}\begin{Bmatrix}\chi_1\\ \chi_2\\ \chi_3\\ \zeta^e\\ \zeta^m\end{Bmatrix}\equiv\Gamma_h\chi \tag{46}$$

where Γ_h is an operator matrix and χ is a column matrix containing the components of the fluctuation functions. If we discretize χ using the finite elements as

$$\chi(x_i;y_i)=S(y_i)\boldsymbol{X}(x_i) \tag{47}$$

where S representing the shape functions (in assemble sense excluding the constrained node and slave nodes) and $\boldsymbol{X}$ column matrix of the nodal value of the fluctuation functions for all active nodes. Substituting Eqs. (46) and (47) into Eq. (45), we obtain a discretized version of the functional as

$$\begin{aligned}\Pi_\Omega=\frac{1}{2\Omega}\Big(&\boldsymbol{X}^{\mathrm T}E\boldsymbol{X}+2\boldsymbol{X}^{\mathrm T}D_{h\varepsilon}\Delta\overline{\mathrm Y}+\Delta\overline{\mathrm Y}^{\mathrm T}D_{\varepsilon\varepsilon}\Delta\overline{\mathrm Y}+2\boldsymbol{X}^{\mathrm T}D_{h\theta}\Delta\theta(t)\\&+2\Delta\overline{\mathrm Y}^{\mathrm T}D_{\varepsilon\theta}\Delta\theta(t)+2\boldsymbol{X}^{\mathrm T}D_{hc}+2\Delta\overline{\mathrm Y}^{\mathrm T}D_{\varepsilon C}+D_{\psi\psi}\Delta\theta(t)\\&+D_{\theta\theta}\frac{\Delta\theta(t)^2}{T_0}+D_{CC}\Big)\end{aligned} \tag{48}$$

where

$$E=\int_{\Omega}(\Gamma_h S)^{\mathrm{T}}\mathrm{R}(\Gamma_h S)d\Omega \quad D_{h\varepsilon}=\int_{\Omega}(\Gamma_h S)^{\mathrm{T}}\mathrm{R}d\Omega$$
$$D_{\varepsilon\varepsilon}=\int_{\Omega}Rd\Omega \quad D_{h\theta}=\int_{\Omega}(\Gamma_h S)^{\mathrm{T}}\eta d\Omega$$
$$D_{\varepsilon\theta}=\int_{\Omega}\eta d\Omega \quad D_{hC}=\int_{\Omega}(\Gamma_h S)^{\mathrm{T}}\mathcal{K}d\Omega$$
$$D_{\psi\psi}=\int_{\Omega}Gd\Omega \quad D_{\varepsilon C}=\int_{\Omega}\mathcal{K}d\Omega$$
$$D_{\theta\theta}=\int_{\Omega}c_v d\Omega \quad D_{CC}=\int_{\Omega}h_v d\Omega \tag{49}$$

Minimizing Π_{Ω} in Eq. (48), we obtain the following linear system:

$$E\boldsymbol{X}=-D_{h\varepsilon}\Delta\overline{\mathbf{Y}}-D_{h\theta}\Delta\boldsymbol{\theta}-D_{hC} \tag{50}$$

The fluctuation function $\boldsymbol{X}$ is linearly proportional to $\Delta\overline{Y}$ and $\Delta\theta$, which means the solution can be written as

$$\boldsymbol{X}=\chi_0\Delta\overline{\mathbf{Y}}+\chi_\theta\Delta\boldsymbol{\theta}+\chi_C \tag{51}$$

Substituting Eq. (51) into Eq. (48), we can calculate the free energy density of the UC as

$$\Pi_{\Omega}=\frac{1}{2}\Delta\overline{Y}^{\mathrm{T}}R^*\Delta\overline{Y}+\Delta\overline{Y}^{\mathrm{T}}\eta^*\Delta\theta(t)+\Delta\overline{Y}^{\mathrm{T}}\mathcal{K}^*+\frac{1}{2}G^*\Delta\theta(t)+\frac{1}{2}c_v^*\frac{\Delta\theta(t)^2}{T_0}+\frac{1}{2}h_v^* \tag{52}$$

with

$$R^*=\frac{1}{\Omega}(\chi_0^{\mathrm{T}}D_{h\varepsilon}+D_{\varepsilon\varepsilon})$$
$$\eta^*=\frac{1}{\Omega}\left[\frac{1}{2}\left(D_{h\varepsilon}^{\mathrm{T}}\chi_{\boldsymbol{\theta}}+\chi_0^{\mathrm{T}}D_{h\theta}\right)+D_{\varepsilon\theta}\right]$$
$$\mathcal{K}^*=\frac{1}{\Omega}\left[\frac{1}{2}\left(D_{h\varepsilon}^{\mathrm{T}}\chi_{\mathbf{C}}+\chi_0^{\mathrm{T}}D_{hC}\right)+D_{\varepsilon C}\right]$$
$$G^*=\frac{1}{\Omega}[\chi_C^{\mathrm{T}}D_{h\theta}+\chi_\theta^{\mathrm{T}}D_{hC}+D_{\psi\psi}]$$
$$c_v^*=\frac{1}{\Omega}(\chi_\theta^{\mathrm{T}}D_{h\theta}T_0+D_{\theta\theta})$$
$$h_v^*=\frac{1}{\Omega}(\chi_C^{\mathrm{T}}D_{hC}+D_{CC}) \tag{53}$$

where R^* is a 12×12 effective material matrix containing instantaneous multiphysics material properties; η^* is a 12×1 effective matrix containing the effective instantaneous second order thermal stress tensor β_{ij}^*, the effective pyroelectric vector p_i^* and the effective pyromagnetic vector m_i^*; $\mathcal{K}^*$is a 12×1 effective matrix containing the effective instantaneous second order tensor ω_{ij}^*, the effective vector ϖ_i^* and the effective vector Ψ_i^*.

After having uniquely determined the fluctuation functions, we can recover the local displacement, electric potential, and magnetic potential as

$$\begin{Bmatrix}\Delta u_1\\ \Delta u_2\\ \Delta u_3\\ \Delta\varnothing^e\\ \Delta\varnothing^m\end{Bmatrix}=\begin{Bmatrix}\Delta v_1\\ \Delta v_2\\ \Delta v_3\\ \Delta\varphi^e\\ \Delta\varphi^m\end{Bmatrix}+\begin{bmatrix}\frac{\partial\Delta v_1}{\partial x_1} & \frac{\partial\Delta v_1}{\partial x_2} & \frac{\partial\Delta v_1}{\partial x_3}\\ \frac{\partial\Delta v_2}{\partial x_1} & \frac{\partial\Delta v_2}{\partial x_2} & \frac{\partial\Delta v_2}{\partial x_3}\\ \frac{\partial\Delta v_3}{\partial x_1} & \frac{\partial\Delta v_3}{\partial x_2} & \frac{\partial\Delta v_3}{\partial x_3}\\ \frac{\partial\Delta\varphi^e}{\partial x_1} & \frac{\partial\Delta\varphi^e}{\partial x_2} & \frac{\partial\Delta\varphi^e}{\partial x_3}\\ \frac{\partial\Delta\varphi^m}{\partial x_1} & \frac{\partial\Delta\varphi^m}{\partial x_2} & \frac{\partial\Delta\varphi^m}{\partial x_3}\end{bmatrix}\begin{Bmatrix}y_1\\ y_2\\ y_3\end{Bmatrix}+\overline{S}\hat{\boldsymbol{X}} \tag{54}$$

where $\overline{S}$ is different from S and $\hat{\boldsymbol{X}}$ is different from $\boldsymbol{X}$ due to the recovery of slave nodes and the constrained node. The increments of the local strain field, local electrical field, and local magnetic field can be recovered as

$$\Delta Y=\Delta\overline{Y}+\Gamma_h\overline{S}\hat{\boldsymbol{X}} \tag{55}$$

Finally, the increments of the increments of the local stress field, electrical displacement field, and magnetic flux density can be recovered straightforwardly using the 3D constitutive relations for the constituent material as

$$\Delta X=R\Delta Y+\eta\Delta\theta(t)+\mathcal{K} \tag{56}$$

The simulations of the time-dependent and non-linear thermo-electro-magneto-viscoelastic-plastic response of smart composites are performed using an incremental procedure based on Eq. (19). Once the R^*, η^*, and $\mathcal{K}^*$ have been determined at the current mechanical loading, electrical charge, or magnetic charge, one can determine the current values of variables from previous values and increments according to

$$\overline{X}_{current}=\overline{X}_{previous}+\Delta\overline{X} \tag{57a}$$

$$\overline{Y}_{current}=\overline{Y}_{previous}+\Delta\overline{Y} \tag{57b}$$

The simulations can be readily performed without applying various boundary conditions as those are carried out using finite element unit cell procedures.

4. Numerical examples

4.1. Material properties of constituents

Aluminum: The material properties of aluminum are presented in Table 1. The mechanical behavior of the aluminum is described using rate-independent elasto-plastic model expressed in Eqs. (10) and (11). Isotropic linear hardening is assumed for the aluminum.

Piezoelectric and Piezomagnetic material: Table 2 presents the material properties of piezoelectric material ($BaTiO_3$) and piezomagnetic material ($CoFe_2O_4$).

Polymer: The polymer is assumed to be isotropic and linear viscoelastic materials. The elastic relaxation modulus of the polymer

Table 1
Material properties of aluminum core.

Young's modulus E (MPa)	Poisson's ratio ν	Yielding strength σ_Y (MPa)	Hardening modulus E_T (MPa)	CTE α (1/°C)	Dielectric coefficient k (C/V m)
70,000	0.33	10	1170	23.0×10^{-6}	0.1×10^{-9}

Table 2
Material properties of the composite constituents ($BaTiO_3$ and $CoFe_2O_4$) [14,15].

	$BaTiO_3$ (piezoelectric)	$CoFe_2O_4$ (piezomagnetic)
C_{11} (GPa)	162	269.5
C_{12} (GPa)	78	170
C_{23} (GPa)	77	173
C_{22} (GPa)	166	286
C_{55} (GPa)	43	45.3
k_{11} (C/V m)	12.6×10^{-9}	0.093×10^{-9}
k_{33} (C/V m)	11.2×10^{-9}	0.08×10^{-9}
μ_{11} (N s^2/C^2)	0.1×10^{-4}	1.57×10^{-4}
μ_{33}(N s^2/C^2)	0.05×10^{-4}	-5.9×10^{-4}
e_{11} (C/m^2)	18.6	0
e_{21} (C/m^2)	−4.4	0
e_{51} (C/m^2)	11.6	0
q_{11} (N/A m)	0	699.7
q_{21} (N/A m)	0	580.3
q_{51} (N/A m)	0	550
α_{11} (1/°C)	6.4×10^{-6}	10×10^{-6}
α_{22} (1/°C)	15.7×10^{-6}	10×10^{-6}
α_{33} (1/°C)	15.7×10^{-6}	10×10^{-6}

can be expressed using Prony series as

$$E(t)=E_0\left(1-\sum_{k=1}^{n}g_k\left(1-e^{-t/\tau_k}\right)\right) \tag{58}$$

where E_0 is the instantaneous Young's modulus; g_k is dimensionless modulus and τ_k is the time relaxation material parameter. For simplicity, we considered a special case, namely, $n=1$, $g_1=0.5$, and $\tau_1=30$, such that Eq. (58) is reduced to

$$E(t)=0.5E_0\left(1+e^{-t/\rho}\right)=A+Be^{-t/\rho} \tag{59}$$

where $E_0=8000$ MPa and $\rho=30$, then $A=B=4000$ MPa. The dielectric coefficient and magnetic permeability of the polymer are assumed to be constant and assigned as $k=0.1\times10^{-9}$ C/(Vm) and $\mu=0.01\times10^{-4}$ Ns^2/C^2, respectively. The thermal expansion of the polymer material are kept constant as $\alpha=54\times10^{-6}$ °C^{-1}.

The time-scale shift factor a_T in Eq. (3) is determined by empirical relationship of Williams–Landel–Ferry (WLF) [19],

$$\log\ a_T(T)=-\frac{C_1(T-T_0)}{C_2+(T-T_0)} \tag{60}$$

where C_1 and C_2 are material constants determined through least squares fitting. In this example, the values of C_1 and C_2 are set as $C_1=4.92$ and $C_2=215.0$.

T_0 in Eq. (60) is the reference temperature and the temperature T at time t is given by

$$T=T_0+\theta=T_0+C_0t \tag{61}$$

where C_0 is the temperature change rate.

Therefore, the reduced time $\xi(t+\Delta t)$, $\xi(t)$, and $\xi(\tau)$ are given by

$$\begin{aligned}\xi(t+\Delta t)&=\int_0^{t+\Delta t}10^{\frac{C_1C_0t'}{C_2+C_0t'}}dt'\\ \xi(t)&=\int_0^{t}10^{\frac{C_1C_0t'}{C_2+C_0t'}}dt'\\ \xi(\tau)&=\int_0^{\tau}10^{\frac{C_1C_0t'}{C_2+C_0t'}}dt'\end{aligned} \tag{62}$$

The stress relaxation stiffness matrix $[L_{ijkl}(t)]$ in Eq. (7a) is obtained as

$$[L_{ijkl}(t)]=ff[W] \tag{63}$$

where the coefficient ff is computed using Simpson's rule of numerical integration as

$$ff=\frac{t}{6}(fL+4fm+fu) \tag{64}$$

where

$$\begin{aligned}fL&=A+Be^{-\frac{\xi(t+\Delta t)-\xi(t)}{\rho}}\\ fu&=A+B\\ fm&=A+Be^{-\frac{\xi(t+\Delta t)-\xi(t/2)}{\rho}}\end{aligned}$$

The matrix$[W]$ in Eq. (63) is given by

$$[W]=\frac{1}{(1+\nu)(1-2\nu)}\begin{bmatrix}1-\nu & \nu & \nu & & & & 0 & 0 & 0\\ \nu & 1-\nu & \nu & & & & 0 & 0 & 0\\ \nu & \nu & 1-\nu & & & & 0 & 0 & 0\\ 0 & 0 & 0 & (1-2\nu)/2 & 0 & 0 & & & \\ 0 & 0 & 0 & 0 & (1-2\nu)/2 & 0 & & & \\ 0 & 0 & 0 & 0 & 0 & (1-2\nu)/2 & & & \end{bmatrix} \tag{65}$$

with ν being the Poisson's ratio of the polymer, which is assumed to be constant $\nu=0.4$.

The matrix $[\gamma_{ij}(t)]$ in Eq. (7a) is obtained as

$$[\gamma_{ij}(t)]=[L_{ijkl}(t)]\{\alpha\} \tag{66}$$

where $\{\alpha\}$ is a column matrix containing thermal expansion coefficients of the polymer materials.

The coefficient matrix of $\omega_{ij}(t)$ in Eq. (7a) is calculated as

$$\begin{aligned}[\omega_{ij}(t)]=\frac{B}{\Delta t}\sum_{i=1}^{n}\Bigg\{&\left(\int_{(i-1)\Delta t}^{i\Delta t}\left(e^{-(t+\Delta t-\tau)/\rho}-e^{-(t-\tau)/\rho}\right)[W]d\tau\right)[\Delta\varepsilon(i)]\\ &+\left(\int_{(i-1)\Delta t}^{i\Delta t}\left(e^{-(t+\Delta t-\tau)/\rho}-e^{-(t-\tau)/\rho}\right)[W]d\tau\right)\{\alpha\}\Delta\theta(i)\Bigg\}\end{aligned} \tag{67}$$

where $[\Delta\varepsilon(i)]$ is 6×1 column matrix containing strain increments during the ith time step Δt; $\Delta\theta(i)$ are the increment of temperature change during the ith time step Δt; and $n=t/\Delta t$.

4.2. Model verification

Let us firstly calculate the stress–strain hysteresis loop of the polymer matrix using VAMUCH and ABAQUS. The polymer was simultaneously applied with cyclic stress loading and various temperature changes as shown in Fig. 2. The temperature changes increase linearly and uniformly up to 20 °C, 40 °C, 60 °C, and 80 °C, respectively. The corresponding responses of the polymer are illustrated in Fig. 3 in which the stress–strain hysteresis loop of the polymer without thermal effects is also plotted for the sake of comparison. Since the VAMUCH predictions are identical to ABAQUS results, only VAMUCH results are illustrated in Fig. 3 from which one can see that the finally remained strains increase as the temperature changes increase after reverse unloading.

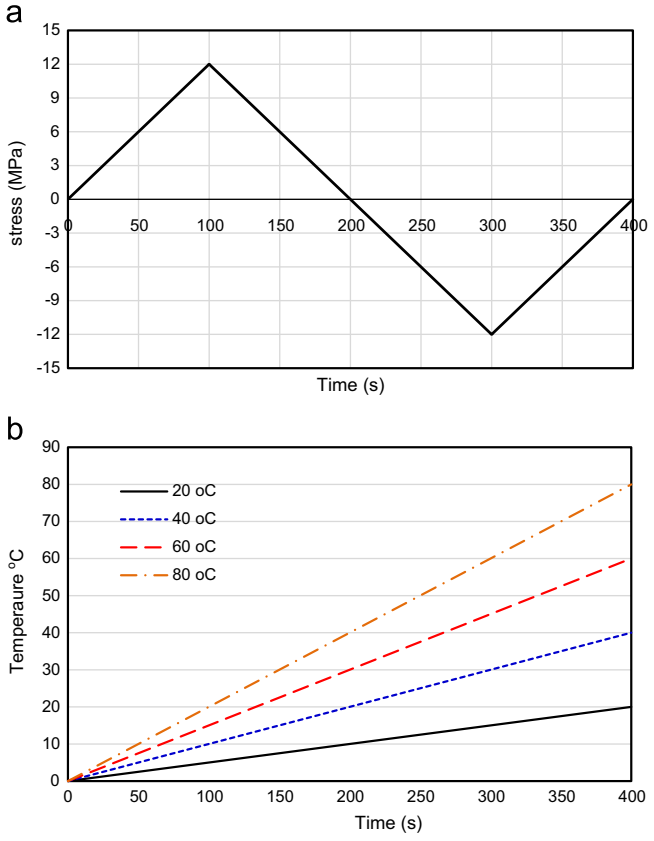

Fig. 2. (a) Cyclic stress loading and (b) temperature changes increase linearly and uniformly up to 20 °C, 40 °C, 60 °C, and 80 °C, respectively, during cyclic stress loading.

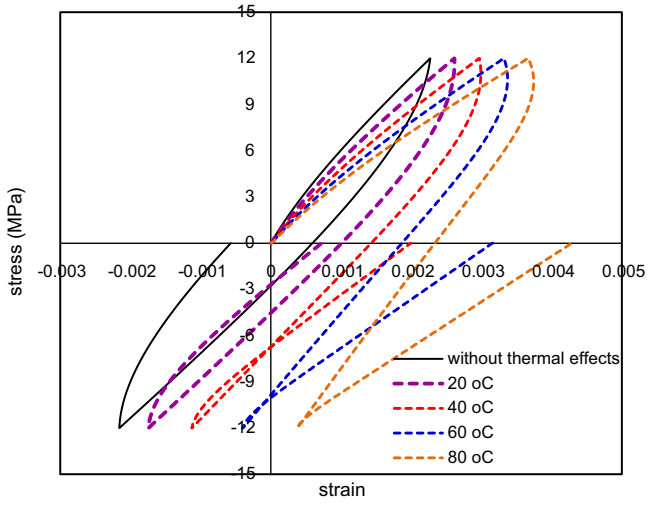

Fig. 3. Predicted uniaxial stress–strain hysteresis curves of linear viscoelastic polymer when the cyclic stress loading and temperature change were applied simultaneously.

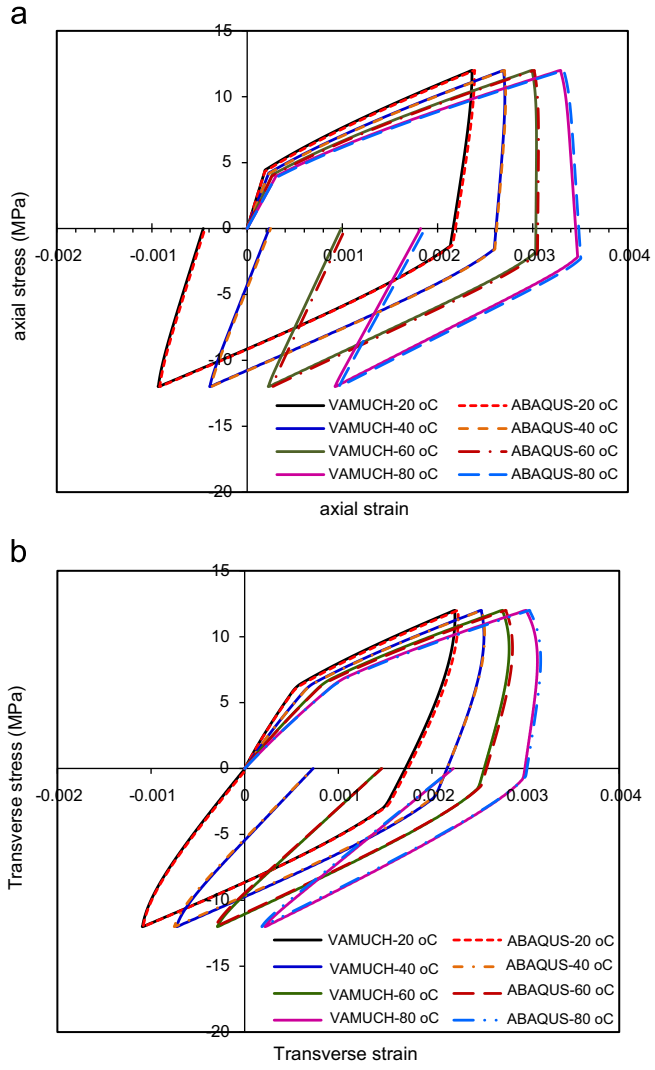

Fig. 4. Uniaxial global stress–strain hysteresis loops of aluminum fiber reinforced composites subjected to couple various temperature changes and: (a) longitudinal cyclic loading $\bar{\sigma}_{11}$ *vs* $\bar{\varepsilon}_{11}$ and (b) transverse cyclic loading $\bar{\sigma}_{22}$ *vs* $\bar{\varepsilon}_{22}$.

Let us consider an aluminum fiber reinforced polymer matrix composites with the volume fraction of aluminum fiber being vof=0.4. The aluminum fiber is of circular shape and in square array. The composite is simultaneously applied with the cyclic stress loading (along fiber direction and transverse direction, respectively) and various temperature changes as shown in Fig. 2. The stress–strain hysteresis curves of aluminum fiber polymer matrix composite due to axial and transverse cyclic loadings coupled with temperature change are plotted in Fig.4 from

which one can observe that there are excellent agreements between the predictions of VAMUCH and ABAQUS.

Next consider a piezoelectric ($BaTiO_3$) fiber reinforced aluminum matrix composite with the volume fraction of $BaTiO_3$ fiber being vof=0.4. The composite was simultaneously applied with temperature changes shown in Fig. 2(b) and electrical field $\bar{E}_1$ along the fiber direction. Fig. 5 shows the variation of the effective induced axial strain $\bar{\varepsilon}_{11}$ of traction-free piezoelectric ($BaTiO_3$) fiber reinforced aluminum matrix composite with the applied electrical field $\bar{E}_1$ at various temperature changes. It can be seen that VAMUCH and ABAQUS provide identical predictions. VAMUCH can also accurately recover the local fields based on the global responses and the recovery relations obtained from the micromechanics analysis. Fig. 6 illustrates the contour plot of local stress component σ_{22} (predicted by VAMUCH) and the comparison of the distributions of σ_{22} along the y_2 axis predicted by VAMUCH and ABAQUS. The results were calculated when the electrical field $\bar{E}_1$ and temperature change increased up to 1.96 MV/m and 60 °C, respectively. One can see from Fig. 6 that the recovery capability of VAMUCH is validated by ABAQUS results.

4.3. *Effective responses of aluminum core piezoelectric and piezomagnetic fiber (APPF) composites*

In this section, the effective responses of aluminum core piezoelectric and piezomagnetic fiber (APPF) reinforced polymer matrix composite whose microstructure is shown in Fig. 7 were investigated using VAMUCH. The volume fractions of polymer matrix, aluminum core, and piezoelectric material are 0.55, 0.3, and 0.05, respectively.

We firstly considered the effects of strain rates on the uniaxial tension behavior. Fig. 8 presents the effective uniaxial tension stress–strain curves of APPF reinforced polymer matrix composite at various strain rates while all electrical fields and magnetic fields

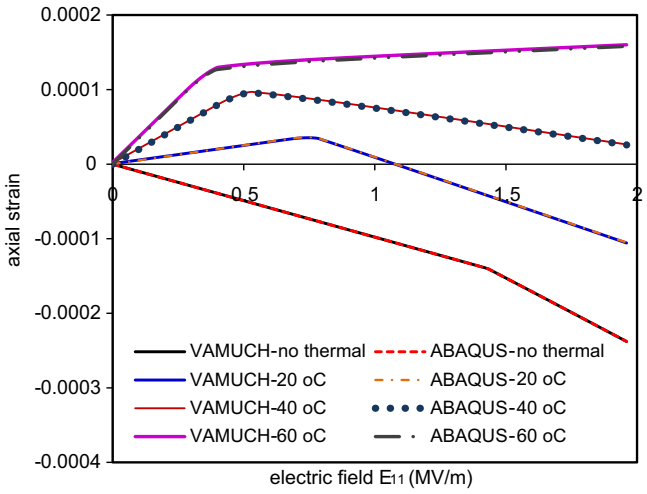

Fig. 5. The effective induced axial strain $\bar{\varepsilon}_{11}$ of traction-free piezoelectric ($BaTiO_3$) fiber reinforced aluminum matrix composite versus the applied electrical field $\bar{E}_1$ at various temperature changes.

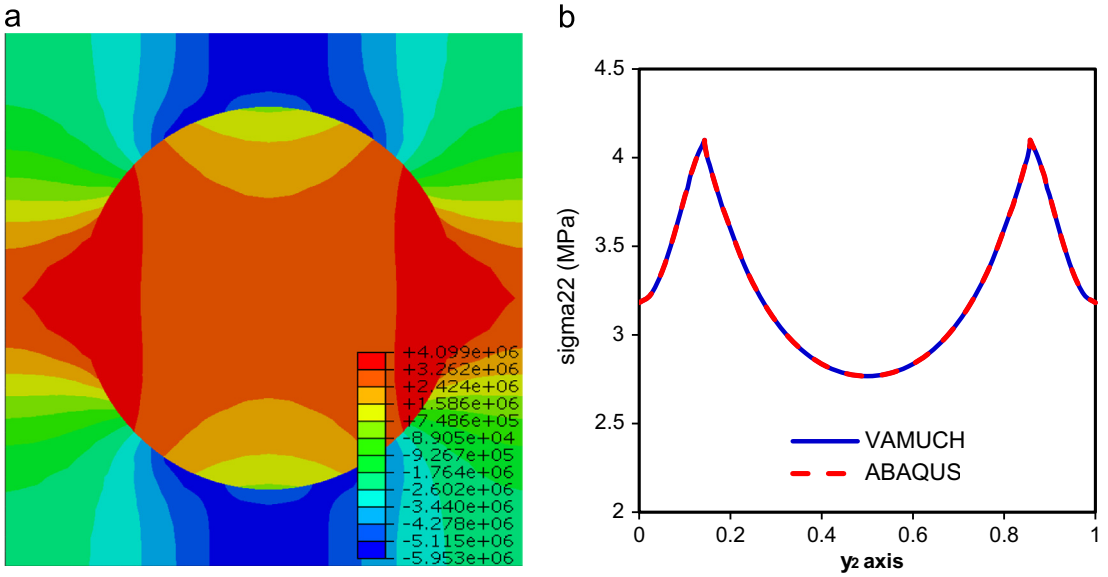

Fig. 6. The recovered local stress of piezoelectric ($BaTiO_3$) fiber reinforced aluminum matrix composite: (a) Contour plot of stress component σ_{22} (Pa) and (b) the distribution of σ_{22} along the y_2 axis.

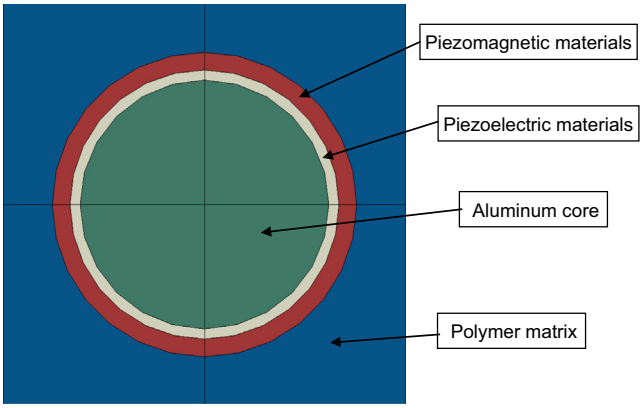

Fig. 7. Microstructure of smart composites consisting of aluminum core, piezomagnetic material, piezoelectric material, and polymer matrix.

are kept zero. Obviously, the tension behaviors of the composite are rate dependent due to the time dependent behavior of the polymer matrix while the influences of strain rates are more pronounced on the transverse tension than on axial tension.

Let us consider the thermal induced axial stress $\bar{\sigma}_{11}$ of APPF polymer matrix composites when all mechanical strains, electric fields, and magnetic fields are kept as zero. This is shown in Fig. 9, which demonstrates that the magnitude of induced axial stress increases with the increase of the temperature change rate. The variation of slope of the curve of induced stress $\bar{\sigma}_{11}$ vs temperature change is due to the modulus relaxation of the polymer matrix.

When all mechanical strains are equal to zero, the induced axial stresses $\bar{\sigma}_{11}$ of APPF polymer matrix composites are generated by axial electric field $\overline{E}_1$ and axial magnetic field $\overline{H}_1$ are presented in Figs. 10 and 11, respectively. It can be seen that the rate of $\overline{E}_1$ and $\overline{H}_1$ do not have significant influences on the induced longitudinal overall stress $\bar{\sigma}_{11}$.

The deformation of smart composites induced by electric input can be utilized for sensoring applications. Figs. 12 and 13 illustrate such responses of traction free APPF reinforce polymer matrix

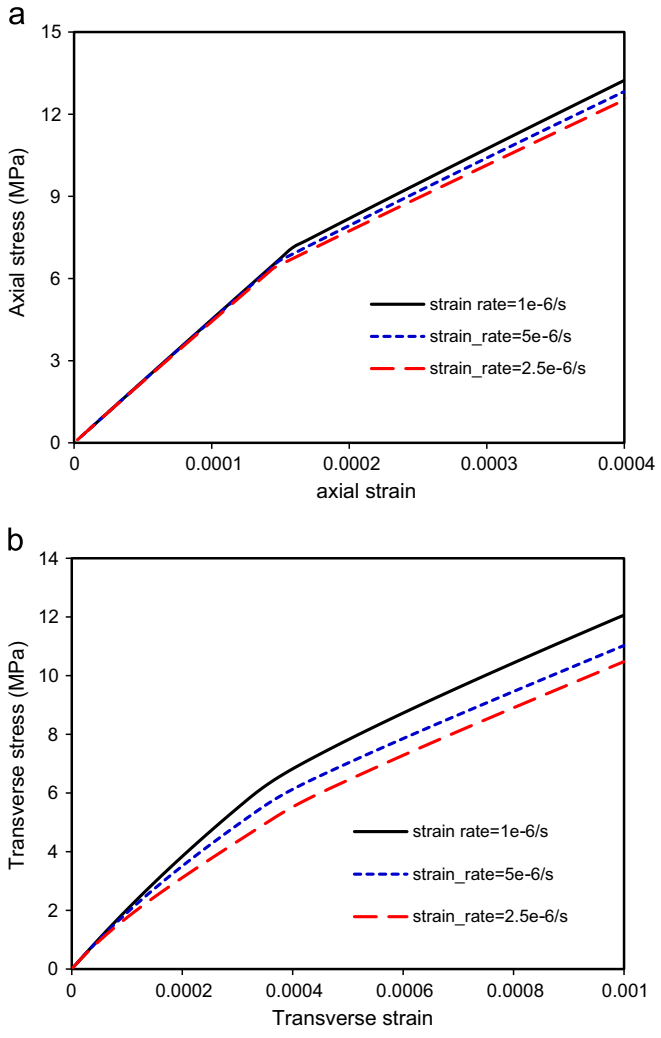

Fig. 8. Effective uniaxial tension stress–strain curves of APPF reinforced polymer matrix composite at various strain rates while all electrical fields and magnetic fields are kept zero: (a) axial tension $\bar{\sigma}_{11}$ *vs* $\bar{\varepsilon}_{11}$ and (b) transverse tension $\bar{\sigma}_{22}$ *vs* $\bar{\varepsilon}_{22}$.

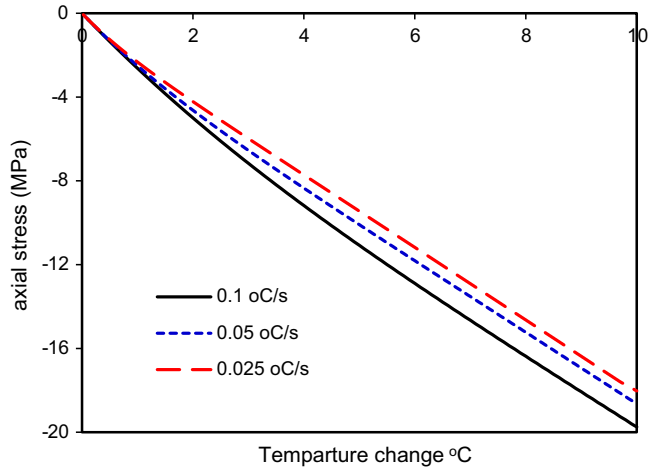

Fig. 9. Induced axial stress $\overline{\sigma}_{11}$ of APPF polymer matrix composite due to the temperature change at three different temperature change rates while all mechanical strains, electric fields, and magnetic fields are kept zero.

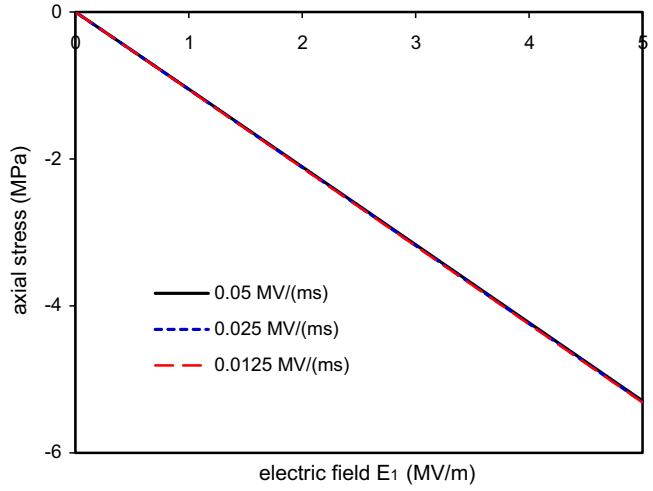

Fig. 10. Induced axial stress $\overline{\sigma}_{11}$ of APPF polymer matrix composite due to the electric field $\overline{E}_1$ at three different electric field rates while all mechanical strains, other components of electric fields, and magnetic fields are kept zero.

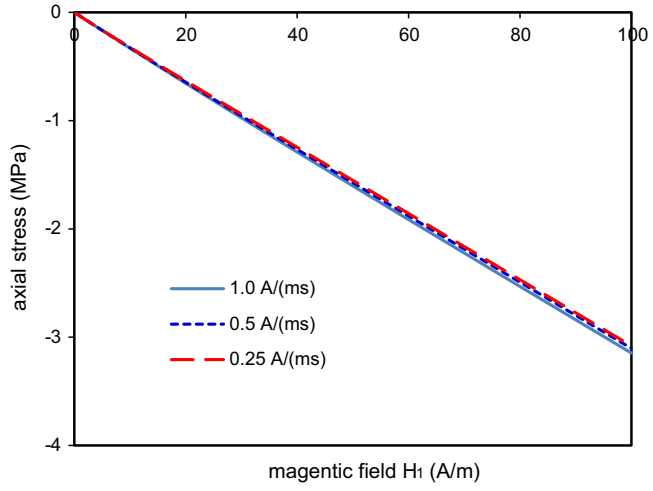

Fig. 11. Induced axial stress $\overline{\sigma}_{11}$ of APPF polymer matrix composite due to the magnetic field $\overline{H}_1$ at three different magnetic field rates while all mechanical strains, other components of magnetic fields, and electric fields are kept zero.

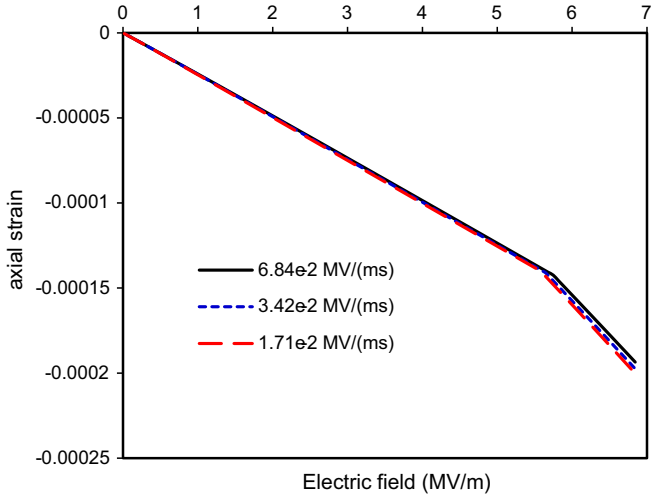

Fig. 12. The effective induced axial strain $\overline{\varepsilon}_{11}$ of traction-free APPF reinforced polymer matrix composites versus the applied electric field $\overline{E}_1$ for three different electric field rates.

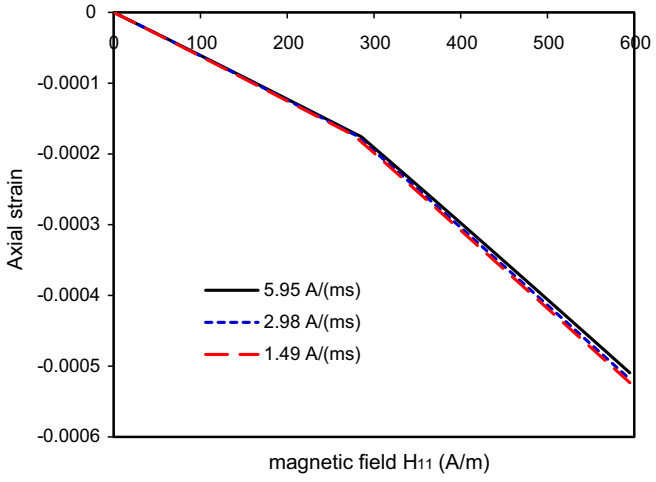

Fig. 13. The effective induced axial strain $\overline{\varepsilon}_{11}$ of traction-free APPF reinforced polymer matrix composites versus the applied magnetic field $\overline{H}_1$ for three different magnetic field rates.

composites. These two figures also clearly illustrate that the yielding of aluminum core causes the change of the slope of the lines of $\overline{\varepsilon}_{11}$ vs $\overline{E}_1$ and $\overline{\varepsilon}_{11}$ vs $\overline{H}_1$ when the axial electrical field $\overline{E}_1$ and axial magnetic field $\overline{H}_1$ increased up to certain values.

5. Conclusions

We have developed a general-purpose micromechanical model that is capable of predicting the fully coupled thermo-electro-magneto-viscoelastic-plastic response of smart composites. In view of the time dependent characteristics and non-linearity of the composite, instantaneous tangential electro-magneto-mechanical matrices associated with an incremental procedure were established. The proposed model can efficiently capture the rate-dependent and non-linear behavior of multiphase smart composite consisting of linear viscoelastic materials, piezoelectric materials, piezomagnetic materials, and metallic phases.

References

[1] A. Van Run, D. Terrell, J. Scholing, An in situ grown eutectic magnetoelectric composite materials, J. Mater. Sci. 9 (1974) 1710–1714.

[2] C.W. Nan, Magnetoelectric effect in composites of piezoelectric and piezomagnetic phases, Phys. Rev. B. 50 (1994) 6082–6088.
[3] G. Harshe, J.P. Dougherty, R.E. Newnham, Theoretical modeling of 3–0/0–3 magneto-electric composite, Int. J. Appl. Electromagn. Mater. 4 (1993) 161–171.
[4] M. Avellaneda, G. Harshe, Magnetoelectric effect in piezoelectric/magnetostrictive multilayer (2–2) composites, J. Intell. Mater. Syst. Struct. 5 (1994) 501–513.
[5] Y. Benveniste, Magnetoelectric effect in fibrous composites with piezoelectric and piezomagnetic phases, Phys. Rev. B 51 (1995) 16424–16427.
[6] J.H. Huang, Analytical predictions for the magnetoelectric coupling in piezomagnetic materials reinforced by piezoelectric ellipsoidal inclusions, Phys. Rev. B 58 (1998) 12–15.
[7] T.L. Wu, J.H. Huang, Closed-form solutions for the magneto-electric coupling coefficients in fibrous composites with piezoelectric and piezomagnetic phases, Int. J. Solids Struct. 37 (2000) 2981–3009.
[8] J.H. Huang, H.K. Liu, W.L. Dai, The optimized fiber volume fraction for magneto-electric coupling effect in piezoelectric–piezomagnetic continuous fiber reinforced composites, Int. J. Eng. Sci. 38 (2000) 1207–1217.
[9] J.Y. Li, Magnetoelectroelastic multi-inclusion and inhomogeneity problems and their applications in composite materials, Int. J. Eng. Sci. 38 (2000) 1993–2011.
[10] J.Y. Li, M.L. Dunn, Micromechanics of magnetoelectroelastic composite materials: average fields and effective behavior, J. Intell. Mater. Syst. Struct. 9 (1998) 404–416.
[11] J. Aboudi, Micromechanical analysis of fully coupled electro-magneto-thermoelastic multiphase composites, Smart Mater. Struct. 10 (2001) 867–877.
[12] J.H. Huang, W.S. Kuo, The analysis of piezoelectric/piezomagnetic composite materials containing ellipsoidal inclusions, J. Appl. Phys. 81 (1997) 1378–1386.
[13] B.A. Bednarcyk, An inelastic micro/macro theory for hybrid smart/metal composites, Composites: Part B 34 (2003) 175–197.
[14] R.M. Haj-Ali, A.H. Muliana, A micromechanical constitutive framework for the nonlinear viscoelastic behavior of pultruded composite materials, Int. J. Solids Struct. 40 (2003) 1037–1057.
[15] W. Yu, T. Tang, Variational asymptotic method for unit cell homogenization of periodically heterogeneous materials, Int. J. Solids Struct. 44 (2007) 3738–3755.
[16] A.S. Wineman, K.R. Rajagopal, Mechanical Response of Polymers: An Introduction, Cambridge University Press, New York, 2000.
[17] A.V. Pyatigorets, M.O. Marasteanu, L. Khazanovich, H.K. Stolarski, Application of a matrix operator method to the thermocviscoelastic analysis of composite structures, J. Mech. Mater. Struct. 5 (5) (2010) 837–854.
[18] V.L. Berdichevsky, On averaging of periodic systems, J. Appl. Math. Mech. 41 (6) (1977) 993–1006.
[19] Malcolm L. Williams, Robert F. Landel, John D. Ferry, The temperature dependence of relaxation mechanisms in amorphous polymers and other glass-forming liquids, J. Am. Chem. Soc. **77** (14) (1955) 3701–3707.